Journal of
Composites Science

MDPI

Article

Ab Initio Modelling of *g*-ZnO Deposition on the Si (111) Surface

Aliya Alzhanova [1], Yuri Mastrikov [2] and Darkhan Yerezhep [3,*]

[1] Faculty of Physics and Technology, Department of Technical Physics, L.N. Gumilyov Eurasian National University, 2 Satpayev Str., Nur-Sultan 010000, Kazakhstan; aliya.alzhan@yandex.kz
[2] Institute of Solid State Physics, University of Latvia, 1001-1084 Riga, Latvia; yuri.mastrikov@cfi.lu.lv
[3] Institute of Energy and Mechanical Engineering, Satbayev University, Almaty 050040, Kazakhstan
* Correspondence: darhan_13@physics.kz

Abstract: Recent studies show that zinc oxide (ZnO) nanostructures have promising potential as an absorbing material. In order to improve the optoelectronic properties of the initial system, this paper considers the process of adsorbing multilayer graphene-like ZnO onto a Si (111) surface. The density of electron states for two- and three-layer graphene-like zinc oxide on the Si (111) surface was obtained using the Vienna ab-initio simulation package by the DFT method. A computer model of graphene-like Zinc oxide on a Si (111)-surface was created using the DFT+U approach. One-, two- and three-plane-thick graphene-zinc oxide were deposited on the substrate. An isolated cluster of Zn_3O_3 was also considered. The compatibility of *g*-ZnO with the S (100) substrate was tested, and the energetics of deposition were calculated. This study demonstrates that, regardless of the possible configuration of the adsorbing layers, the Si/ZnO structure remains stable at the interface. Calculations indicate that, in combination with lower formation energies, wurtzite-type structures turn out to be more stable and, compared to sphalerite-type structures, wurtzite-type structures form longer interlayers and shorter interplanar distances. It has been shown that during the deposition of the third layer, the growth of a wurtzite-type structure becomes exothermic. Thus, these findings suggest a predictable relationship between the application method and the number of layers, implying that the synthesis process can be modified. Consequently, we believe that such interfaces can be obtained through experimental synthesis.

Keywords: ZnO; DFT; VASP; Si; nanoclusters; adsorbed; Ab initio; computational modelling; material properties

check for updates

Citation: Alzhanova, A.; Mastrikov, Y.; Yerezhep, D. Ab Initio Modelling of *g*-ZnO Deposition on the Si (111) Surface. *J. Compos. Sci.* **2024**, *8*, 281. https://doi.org/10.3390/jcs8070281

Academic Editor: Zhong Hu

Received: 12 June 2024
Revised: 15 July 2024
Accepted: 17 July 2024
Published: 20 July 2024

Copyright: © 2024 by the authors. Licensee MDPI, Basel, Switzerland. This article is an open access article distributed under the terms and conditions of the Creative Commons Attribution (CC BY) license (https://creativecommons.org/licenses/by/4.0/).

1. Introduction

Graphene-like ZnO (*g*-ZnO) nanostructures are currently being investigated, which are interesting as nanomaterials not only because of their electrical and mechanical properties [1–3] but also because of their interesting structure and morphology [4]. Primarily, zinc oxide is characterized by a wide band gap (3.37 eV), high exciton binding energy (60 MeV) and natural *n*-type electrical conductivity [5,6]. The ZnO nanostructure is one of the safest semiconductor materials and is distinguished by such properties as low toxicity, thermal stability, large specific surface area and high electron mobility, which gives this structure great potential for numerous uses in sensor applications [7–10]. In particular, nanowires [11], nanorods [12], and nanotubes [13] are of interest, which are obtained from nanoparticles, that is, one-dimensional semiconductor nanostructures are given more attention because of their elongated morphology with a large ratio of surface area to their volume [14]. These structures, obtained with the help of ZnO nanoparticles, make these one-dimensional semiconductor materials promising for use in various areas of nanotechnology due to their uniqueness and diverse set of positive characteristics.

To expand the range of application of ZnO, researchers apply various methods of modification of the crystal structure using both experimental and theoretical methods of deposition and alloying with various structures [15–19]. The synthesis of zinc oxide

nanostructures can be carried out by many methods, such as depositing by surface epitaxy [20], the coprecipitation method [21] and chemical bath deposition [22]. Thus, due to the excellent properties of ZnO, many works are devoted to the effect of doping of various molecules on the surface of ZnO. For example, in [23], the influence of manganese doping sites of different depths on the electromagnetic properties of ZnO, which makes it possible to obtain ferromagnetism or antiferromagnetism, is reported. The study in [24] shows the effect of silicon doping on the electrical, optical, and magnetic properties of ZnO. And in [25], the effect of co-doping with carbon and silicon on the optoelectronic properties of ZnO is shown. In addition, silicon plays an important role in the modern semiconductor direction and is an alloying impurity that predominantly occupies cationic positions in $A^{III}B^{V}$ semiconductors to improve their electrical and optical properties [26].

Theoretical methods that save time and resources are potentially of great interest [27–29]. So, in order to study and calculate the adsorption energies of the studied systems, we performed density functional theory (DFT) calculations. DFT is a computational method that uses the fundamental laws of quantum mechanics to calculate the electronic structure of atoms, molecules, and solids [30,31]. This modelling method is widely used to calculate the electronic properties of systems with a multilayer nanostructure and shows good convergence results between the experiment and the DFT computational experiment [32].

To the best of our knowledge, there is no theoretical study of graphene-like ZnO adsorbed by two and three layers on the terminated surface of Si (111). Substantial efforts have been made in studying the process of ZnO growth on Si substrates, experimentally and computationally [33]. Yet, the structural stability of the interface between the materials needs to be investigated further. To examine the deposition of the initial *g*-ZnO layers on the Si (111) surface at the atomistic level, we performed computational modelling of the process.

2. Models and Methods

Modelling of *g*-ZnO/Si (111) interfaces was performed by the DFT + *U* method, as implemented in the computer code VASP5.3 [34]. Core electrons were substituted by the PAW potentials [35], standard version. The PBE [36] exchange-correlation functional was used. The Hubbard correction was applied by the Lichtenstein method [37]. *U* and *J* parameters were chosen, based on other theoretical studies (Table 1).

Table 1. Potential details and Hubbard correction parameters for Si and ZnO.

Potentials			Hubbard Correction			
Element	**Free Electrons**	**Potential Cut-Off Energy, eV**	**Orbital**	***U*, eV**	***J*, eV**	**Source**
Si	$3s^2 3p^2$	245.345	*p*	0	4	[38]
Zn	$3d^{10} 4p^2$	276.723	*d*	10	0	[39,40]
O	$2s^2 2p^4$	400	*p*	7	0	[39,40]

The plane wave basis set was restricted to 400 eV. The Brillouin zone for interface calculations was sampled by the Monkhorst-Pack scheme [41] 4 × 4 × 2. The surface was modelled as the 8-plane (4-layer)-thick slab with the surface cell of 7.53 × 7.53 Å and the vacuum gap of 17 Å. A complete geometry optimization was performed for the Si bulk. The Si (111) unreconstructed surface is considered as a model substrate for adsorption modelling. As was shown experimentally [33], Si can be successfully used for this purpose. The Si slab's optimization as well as the *g*-ZnO plane's deposition, was achieved by keeping the parameters of the surface cell fixed to simulate a rigid substrate. The reference ZnO monolayer was optimized completely (Figure 1), forming a flat (interplanar distance = 0 Å) layer [42].

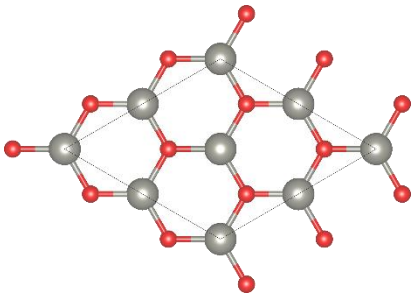

Figure 1. Graphene-like ZnO monolayer: 6.02 × 6.02 Å surface unit (dotted line), four ZnO formula units. Zn-O distance—1.74 Å. Gray and red balls denote Zn and O, respectively.

No vdW interaction was taken into account, although it is beneficial for calculating the absolute energy values [43]. However, the main qualitative conclusions remain the same, since they are based not on the absolute values but on the interactive differences between them (Equation (1)). The energy values are given relative to the structural (surface) units, which makes comparison with other studies straightforward. The surface energy was calculated relative to the bulk and normalized to a 3.76 × 3.76 Å surface unit (or 0.25 of the surface area cell, as shown in Figure 2a).

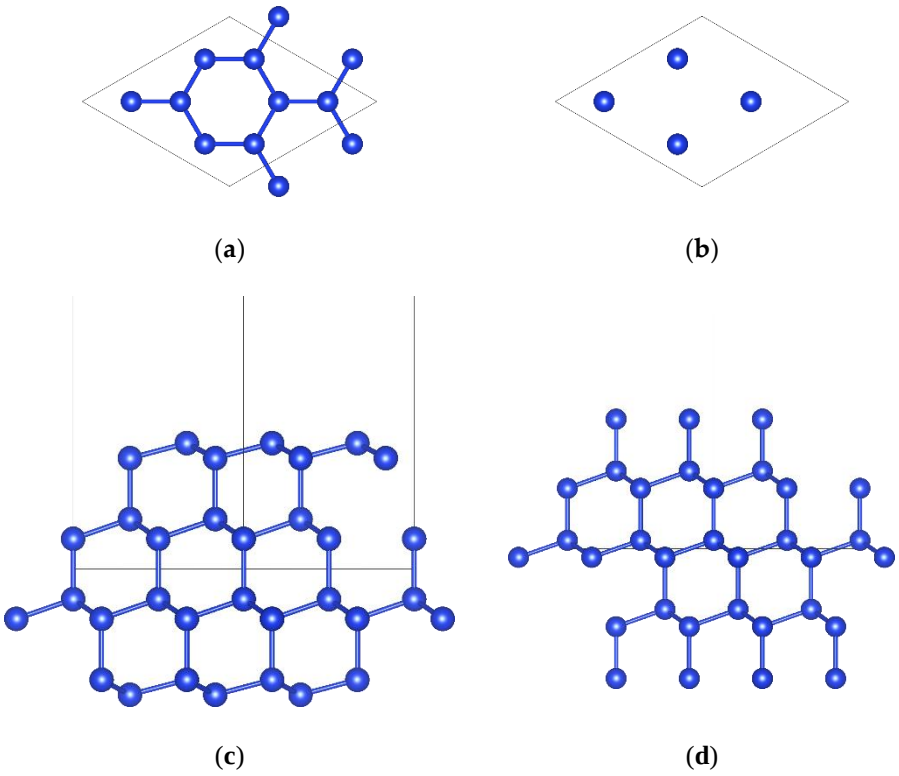

Figure 2. Si (111) slab with closed (**a**,**d**) and open (**b**,**d**) packing. Top (**a**,**b**) (terminating layer only) and side (**c**,**d**) view. The edges of the supercell in the corresponding projections are defined by the lines.

3. Results and Discussion

The Si (111) surface implies the possibility of two terminations—with closed (Figure 2a,c) and open packing (Figure 2b,d)—with surface energies of 1.43 eV/surf.unit (117 meV/Å2) and 2.79eV/surf.unit, which are in good agreement with the value of 124.5 meV/Å from [44]. Therefore, the termination with open packaging, which is energetically very unfavourable, was eliminated from further modelling.

The structure of ZnO, both sphalerite- (Figure 3a) and wurtzite-type (Figure 3b), makes it suitable for a planar deposition on Si substrate.

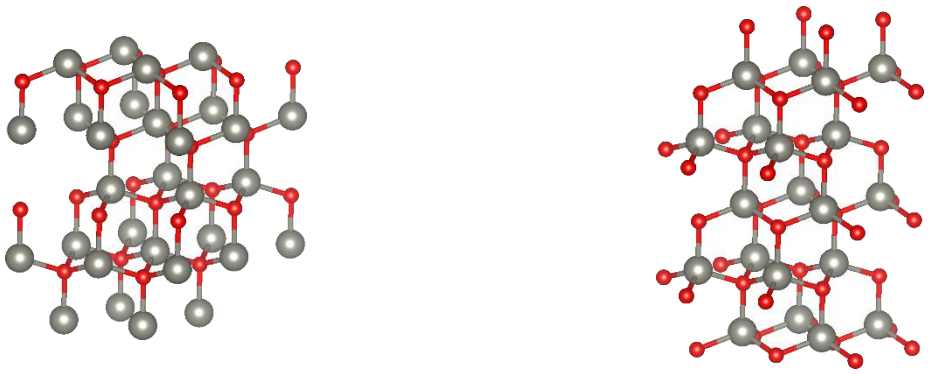

(**a**) (**b**)

Figure 3. Sphalerite (**a**) and wurtzite-type (**b**) ZnO structures. Gray and red balls denote Zn an O, respectively.

The calculated *g*-ZnO formation energy is 0.5 eV per ZnO f.u. The ZnO (111) monolayer lattice constant is 80% of that for the Si (111) surface, which makes the materials compatible. The difference between sphalerite- and wurtzite-type structures is in stacking order (Figure 3). Due to the small difference in energy (<0.03 eV), both types have been considered.

Two types of stacking—sphalerite and wurtzite—have been modelled, relative to the Si and relative to the ZnO surface layer (Figure 4).

The deposition energy of *g*-ZnO has been calculated differentially, relative to the monolayer:

$$E_{+g-\mathrm{ZnO}} = E_{Ng-\mathrm{ZnO}} - \left(E_{(N-1)g-\mathrm{ZnO}} + E_{\mathrm{ML}\ g-\mathrm{ZnO}}\right) \quad (1)$$

where E_{Ng-ZnO}—the energy of the system with N deposited *g*-ZnO layers,

$E_{(N-1)g-ZnO}$—the energy of the system with $(N-1)$ deposited *g*-ZnO layers,

$E_{\mathrm{ML}\ g-ZnO}$—the energy of *g*-ZnO (MonoLayer).

The values have been normalized to the ZnO formula unit in the *g*-ZnO monolayer.

Deposited on the Si (111) surface, the ZnO monolayer was stretched to match the lattice constant of Si. The *g*-ZnO monolayer was deposited with oxygen anions forming bonds with silicon cations. Zn cations have been placed, depending on the type of the interface, atop of the subsurface Si cation (sphalerite-type) (Figure 4a) and atop of the surface Si cations (wurtzite-type) (Figure 4f). In both cases, oxygen formed strong bonds with Si from the surface layer. Due to the lattice constant mismatch, the ZnO monolayer was stretched flat without the gap between the Zn and the O planes as in the bulk (Figure 3). Energetically, it requires 0.12 and 0.04 eV to per ZnO f.u. (Table 2) to deposit the monolayer in sphalerite and wurtzite stacking., which makes the latter type of deposition more likely to occur. Yet, the sphalerite type of adsorption is structurally stable and therefore shall not be completely eliminated. The first *g*-ZnO ML builds an interface between the two materials and provides better sorption conditions (more energetically favourable) for the next layers of ZnO.

Table 2. Adsorption energy of the next *g*-ZnO layer on Si (*g*-ZnO) substrate in eV per ZnO formula unit (Equation (1)).

Si/*g*-ZnO	ZnO	1		2		3	
sphalerite	sphalerite	0.12	Figure 4a	0.56	Figure 4b	0.53	Figure 4c
sphalerite	wurtzite			0.49	Figure 4d	−0.07	Figure 4e
wurtzite	wurtzite	0.04	Figure 4f	0.44	Figure 4g	−0.06	Figure 4h
wurtzite	sphalerite			0.57	Figure 4i	0.52	Figure 4j

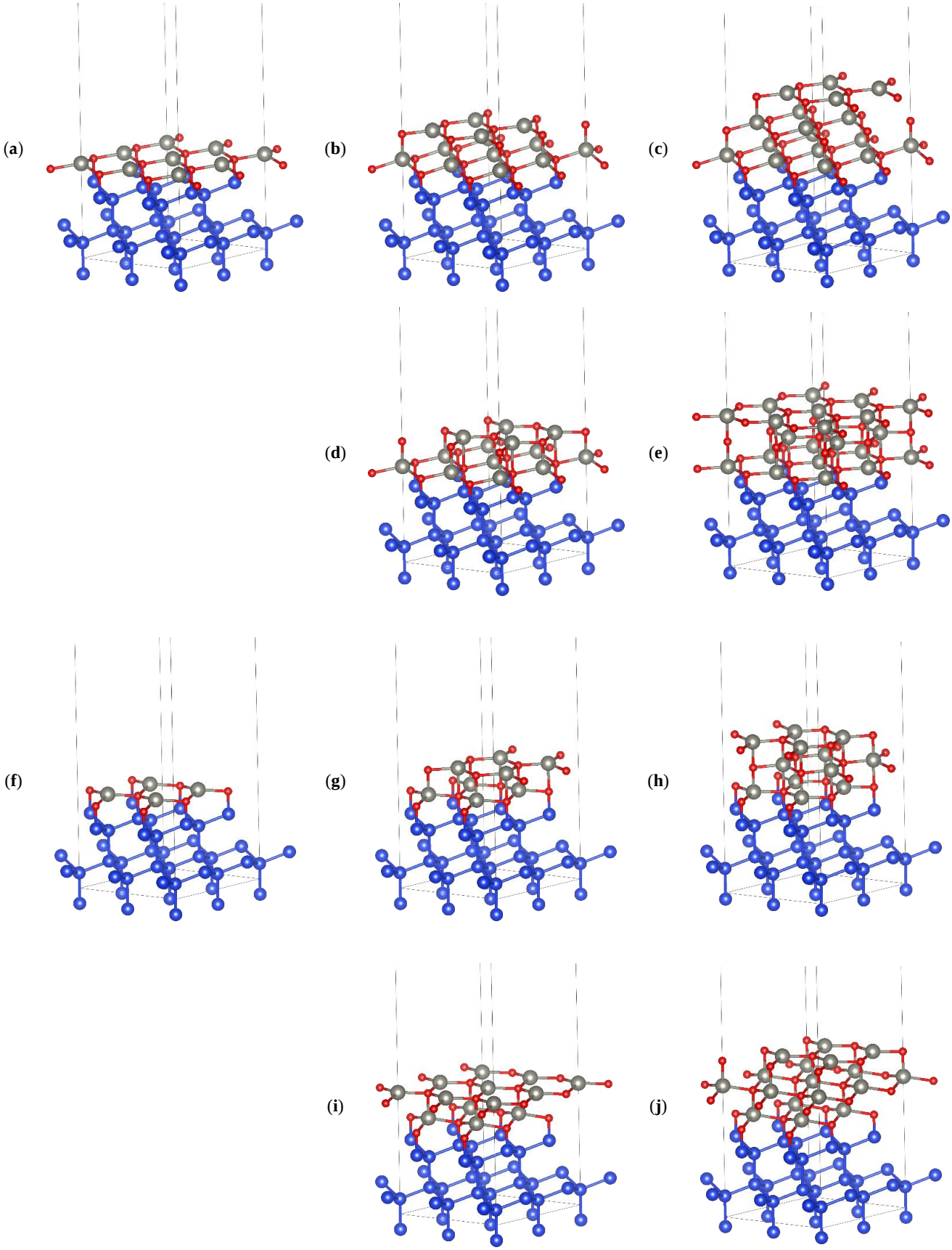

Figure 4. Adsorption of 1 (**a**,**f**), 2 (**b**,**d**,**g**,**i**), and 3 (**c**,**e**,**h**,**j**) *g*-ZnO layers on the Si (111) surface. Sphalerite- (**a**–**e**) and wurtzite-type (**f**–**j**) Si/*g*-ZnO interface.

Two and three ZnO planes were deposited in sphalerite or wurtzite order, relative to the interface ZnO layer. So, total ten stacking combinations were investigated. All of them appeared to be structurally stable.

The smallest Zn-O interplanar was observed in the last deposited layer (exposed to the vacuum) (Table 3, Figure 5a). Wurtzite-type ZnO stacking has, in general, smaller interplanar distances than those of sphalerite type. As the number of deposited ZnO layers grows, the interplanar distance becomes smaller.

Table 3. Interplanar Zn-O (a) and interlayer Si-O and Zn-O distances in *g*-ZnO/Si interfaces (Å). The data are aligned starting from the vacuum.

		Number of ZnO Layers		
Si/ZnO Interface	**ZnO Stacking**	**1**	**2**	**3**
sphalerite	wurtzite		vacuum	
		0.29	0.16	0.15
		1.71	1.86	1.89
		Si	0.62	0.49
			1.69	1.81
			Si	0.61
				1.69
				Si
	sphalerite		vacuum	
			0.07	0.04
			1.86	1.91
			0.38	0.10
			1.72	1.85
			Si	0.05
				1.73
				Si
wurtzite	wurtzite		vacuum	
		0.24	0.04	0.03
		1.71	1.85	1.85
		Si	0.24	0.11
			1.71	1.83
			Si	0.10
				1.73
				Si
	sphalerite		vacuum	
			0.17	0.12
			1.86	1.88
			0.49	0.46
			1.68	1.81
			Si	0.49
				1.68
				Si

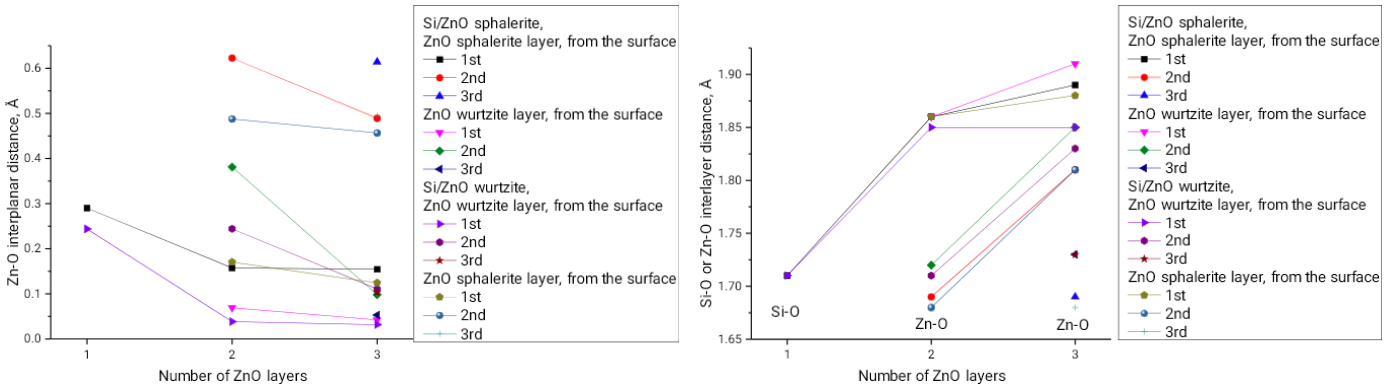

Figure 5. Interplanar (**a**) Zn-O and interlayer (**b**) Si-O and Zn-O distances in *g*-ZnO/Si interfaces. Note that in this analysis ZnO layers are numbered from the surface.

The interlayer distance is the largest in the last deposited ZnO layer. The sphalerite-type Si/ZnO interface demonstrated larger interlayer distances. The interlayer distance increases with the number of deposited ZnO layers (Table 3, Figure 5b).

The energetic analysis of the process reveals that the deposition of the first *g*-ZnO either in sphalerite or wurtzite configuration requires extremely low energy. The deposition of the second layer also requires energy, and the absolute values are below 0.6eV per ZnO f.u. (Figure 6). Overall, the wurtzite ZnO structure is more favourable, which is in agreement with the study [33]. The deposition of the third layer, however, is qualitatively different for wurtzite and sphalerite structures. The former appears to be exothermic, which makes the further deposition self-sustaining.

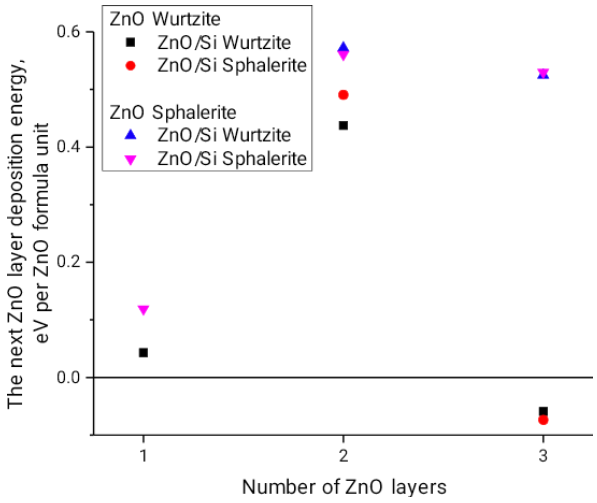

Figure 6. Adhesion energy of ZnO layers deposited on the Si(111) surface.

For reference, the energy levels, relative to ZnO ML (Equation (2)), are listed in Table 4. The energy levels clearly demonstrate the decrease in total energy after the deposition of the third layer of ZnO in the wurtzite-type stacked structure.

$$E_{ref,} = E_{Ng-\mathrm{ZnO}} - \left(E_{\mathrm{Si}} + NE_{\mathrm{ML}g-\mathrm{ZnO}}\right) \quad (2)$$

where $E_{Ng-\mathrm{ZnO}}$ is the energy of the system with N deposited *g*-ZnO layers, E_{Si} is the energy of the substrate, and $E_{\mathrm{ML}\ g-\mathrm{ZnO}}$ is the energy of *g*-ZnO (MonoLayer).

Table 4. Energy states (eV) calculated relative to ZnO monolayer.

Si/ZnO Sphalerite	Number of ZnO Layers	ZnO Stacking	
		Wurtzite	Sphalerite
sphalerite	1	0.12	
	2	0.61	
	3	0.54	
	2		0.68
	3		1.21
wurtzite	1	0.04	
	2	0.48	
	3	0.42	
	2		0.62
	3		1.14

All *g*-ZnO/Si (111) systems appeared to be conducting, which makes such interfaces a promising material for microelectronics. Although the state could be different for thicker systems, in our ultra-thin film model, no band gap was observed.

4. Conclusions

A detailed analysis of *g*-ZnO deposition on the Si (111) ultra-thin film revealed that adsorption of the *g*-ZnO monolayer requires a negligible, small amount of energy. Regardless of the Si/ZnO adsorption configuration, the structure of the interface is stable. In comparison to sphalerite-type stacking, the wurtzite-like one forms longer interlayer and shorter interplanar distances. In combination with lower formation energies, wurtzite-type structures appear to be more stable. Moreover, already at the third layer deposition step, the growth of the wurtzite-type structure becomes exothermic. This indicates a possibility to synthesize such interfaces experimentally.

The present study reveals the key energetic characteristics of a hexagonal-type interface and the process of epitaxial growth of a polymorph material on a structurally compatible substrate. The results of the study suggest that the method of deposition can be changed, depending on the number of deposited layers.

Author Contributions: Conceptualization, A.A. and Y.M.; methodology, A.A. and D.Y.; software, A.A.; validation, A.A., Y.M. and D.Y; formal analysis, A.A., Y.M. and D.Y; investigation, A.A., Y.M. and D.Y.; data curation, A.A. and Y.M.; writing—original draft preparation, A.A., Y.M. and D.Y; writing—review and editing, Y.M. and D.Y; visualization, A.A.; supervision, Y.M.; project administration, Y.M. and D.Y.; funding acquisition, A.A. and D.Y. All authors have read and agreed to the published version of the manuscript.

Funding: This research has been funded by the Science Committee of the Ministry of Science and Higher Education of the Republic of Kazakhstan—«Zhas Galym» 2022/2024 grant No. AP14972733.

Data Availability Statement: Data will be made available upon reasonable request to the corresponding author.

Acknowledgments: A.A. thanks the State Education Development Agency of the Republic of Latvian for the state research scholarship in academic year 2019/2020 (decision No. 1.50.3/2867).

Conflicts of Interest: The authors declare no conflicts of interest.

References

1. Mohamed, K.M.; Benitto, J.J.; Vijaya, J.J.; Bououdina, M. Recent Advances in ZnO-Based Nanostructures for the Photocatalytic Degradation of Hazardous, Non-Biodegradable Medicines. *Crystals* **2023**, *13*, 329. [CrossRef]
2. Sheikhi, S.; Aliannezhadi, M.; Tehrani, F.S. The Effect of PEGylation on Optical and Structural Properties of ZnO Nanostructures for Photocatalyst and Photodynamic Applications. *Mater. Today Commun.* **2023**, *34*, 105103. [CrossRef]
3. Alnaim, N.; Kumar, S.; Alshoaibi, A. Structural, Morphological, Electronic Structural, Optical, and Magnetic Properties of ZnO Nanostructures. *Materials* **2022**, *15*, 8889. [CrossRef] [PubMed]
4. Morandi, S.; Fioravanti, A.; Cerrato, G.; Lettieri, S.; Sacerdoti, M.; Carotta, M.C. Facile Synthesis of ZnO Nano-Structures: Morphology Influence on Electronic Properties. *Sens. Actuators B Chem.* **2017**, *249*, 581–589. [CrossRef]
5. Ayoub, I.; Kumar, V.; Abolhassani, R.; Sehgal, R.; Sharma, V.; Sehgal, R.; Swart, H.C.; Mishra, Y.K. Advances in ZnO: Manipulation of Defects for Enhancing Their Technological Potentials. *Nanotechnol. Rev.* **2022**, *11*, 575–619. [CrossRef]
6. Bhandari, K.P.; Sapkota, D.R.; Jamarkattel, M.K.; Stillion, Q.; Collins, R.W. Zinc Oxide Nanoparticles—Solution-Based Synthesis and Characterizations. *Nanomaterials* **2023**, *13*, 1795. [CrossRef] [PubMed]
7. Ortiz-Casas, B.; Galdámez-Martínez, A.; Gutiérrez-Flores, J.; Baca Ibañez, A.; Kumar Panda, P.; Santana, G.; de la Vega, H.A.; Suar, M.; Gutiérrez Rodelo, C.; Kaushik, A.; et al. Bio-Acceptable 0D and 1D ZnO Nanostructures for Cancer Diagnostics and Treatment. *Mater. Today* **2021**, *50*, 533–569. [CrossRef]
8. Trivedi, S.; Nemade, H.B. ZnO Nanorod-based Love Wave Delay Line for High Mass Sensitivity: A Finite Element Analysis. *IET Sci. Meas. Technol.* **2019**, *13*, 1245–1253. [CrossRef]
9. Ebert, M.; Ghazali, N.A.B.; Kiang, K.S.; Zeimpekis, I.; Maerz, B.; de Planque, M.R.R.; Chong, H.M.H. Multichannel ZnO Nanowire Field Effect Transistors by Lift-off Process. *Nanotechnology* **2018**, *29*, 415302. [CrossRef] [PubMed]
10. Bardakas, A.; Kaidatzis, A.; Tsamis, C. A Review of Magnetoelectric Composites Based on ZnO Nanostructures. *Appl. Sci.* **2023**, *13*, 8378. [CrossRef]
11. Schlur, L.; Calado, J.R.; Spitzer, D. Synthesis of Zinc Oxide Nanorods or Nanotubes on One Side of a Microcantilever. *R. Soc. Open Sci.* **2018**, *5*, 180510. [CrossRef] [PubMed]
12. Del Gobbo, S.; Poolwong, J.; D'Elia, V.; Ogawa, M. Simultaneous Controlled Seeded-Growth and Doping of ZnO Nanorods with Aluminum and Cerium: Feasibility Assessment and Effect on Photocatalytic Activity. *Cryst. Growth Des.* **2020**, *20*, 5508–5525. [CrossRef]
13. Rezaie, M.N.; Mohammadnejad, S.; Ahadzadeh, S. The Impact of ZnO Nanotube on the Performance of Hybrid Inorganic/Organic Light-Emitting Diode as a Single-Mode Ring-Core UV Waveguide. *Surf. Interfaces* **2022**, *28*, 101666. [CrossRef]
14. Real, S.; Espíndola, O.; Zelaya, M.P.; Marin, O.; Comedi, D.; Tirado, M. Single-Step Zno Nanorod Bunches Formation on p-Type Si-Conductive Substrates by Electrophoretic Deposition. *Surf. Interfaces* **2021**, *23*, 100930. [CrossRef]
15. Alshgari, R.A.; Ujjan, Z.A.; Shah, A.A.; Bhatti, M.A.; Tahira, A.; Shaikh, N.M.; Kumar, S.; Ibupoto, M.H.; Elhawary, A.; Nafady, A.; et al. ZnO Nanostructures Doped with Various Chloride Ion Concentrations for Efficient Photocatalytic Degradation of Methylene Blue in Alkaline and Acidic Media. *Molecules* **2022**, *27*, 8726. [CrossRef] [PubMed]
16. Lahmer, M.A. Effect of Doping with Sulfur Atoms on the Electronic and Photocatalytic Properties of the ZnO($10\bar{1}0$) Surface: A DFT+U Study. *Comput. Condens. Matter* **2022**, *31*, e00654. [CrossRef]
17. Vaddadi, V.S.C.S.; Parne, S.R.; Pothukanuri, N.; Sriram, S.R.; Yelsani, V. Investigattions on ZnO Thin Films Modified with Urea: An Approach as Ammonia Sensor. *ACS Omega* **2023**, *8*, 17719–17730. [CrossRef] [PubMed]
18. Zeljković, S.; Balaban, M.; Gajić, D.; Vračević, S.; Ivas, T.; Vranković, D.; Jelić, D. Mechanochemically Induced Synthesis of N-Ion Doped ZnO: Solar Photocatalytic Degradation of Methylene Blue. *Green Chem. Lett. Rev.* **2022**, *15*, 869–880. [CrossRef]
19. Stoltz, K.R.; Echeverria, E.; Kaphle, A.; Austin, A.J.; Harikumar, P.; Yost, A.J.; McIlroy, D.N.; Borunda, M.F. Optimization of the U Parameter in CoO Groupings in ZnO($10\bar{1}0$). *Comput. Mater. Sci.* **2021**, *198*, 110700. [CrossRef]
20. Garratt, E.; Prete, P.; Lovergine, N.; Nikoobakht, B. Observation and Impact of a "Surface Skin Effect" on Lateral Growth of Nanocrystals. *J. Phys. Chem. C* **2017**, *121*, 14845–14853. [CrossRef]
21. Ahmad, S.; Usman, M.; Hashim, M.; Ali, A.; Shah, R.; Rahman, N.U. Investigation of Optical and Dielectric Properties of Nickel-Doped Zinc Oxide Nanostructures Prepared via Coprecipitation Method. *Nanomater. Nanotechnol.* **2024**, *2024*, 8330886. [CrossRef]
22. McPeak, K.M.; Baxter, J.B. ZnO Nanowires Grown by Chemical Bath Deposition in a Continuous Flow Microreactor. *Cryst. Growth Des.* **2009**, *9*, 4538–4545. [CrossRef]
23. Wang, L.-H.; Fu, S.-L.; Wang, C.-A.; Gan, G.-R.; Xie, Y.-P.; Gao, X.-L. The Electromagnetic Properties of ZnO Quantum Dot with Different Mn-Doping Sites. *J. Supercond. Nov. Magn.* **2023**, *36*, 637–646. [CrossRef]
24. Luo, J.T.; Zhu, X.Y.; Chen, G.; Zeng, F.; Pan, F. The Electrical, Optical and Magnetic Properties of Si-Doped ZnO Films. *Appl. Surf. Sci.* **2012**, *258*, 2177–2181. [CrossRef]
25. Said, K.; Baghdad, R. Carbon and Silicon Co-Doping Effect on Microstructural and Optoelectronic Properties of ZnO: An Ab Initio Study. *Optik* **2022**, *260*, 169138. [CrossRef]
26. Mohammadigharehbagh, R.; Özen, S.; Yudar, H.H.; Pat, S.; Korkmaz, Ş. The Electrical, Elemental, Optical, and Surface Properties of Si-Doped ZnO Thin Films Prepared by Thermionic Vacuum Arc. *Mater. Res. Express* **2017**, *4*, 096404. [CrossRef]
27. Zhang, H.; Lu, S.; Xu, W.; Yuan, F. First-Principles Study of Si Atoms Adsorbed on ZnO (0001) Surface and the Effect on Electronic and Optical Properties. *Surf. Sci.* **2014**, *625*, 30–36. [CrossRef]

28. Xu, H.-Y.; Zhang, S.-Q.; Wang, Y.-F.; Xu, Y.; Dong, L.-M.; Komarneni, S. New Insights into the Photocatalytic Mechanism of Pristine ZnO Nanocrystals: From Experiments to DFT Calculations. *Appl. Surf. Sci.* **2023**, *614*, 156225. [CrossRef]
29. Rojas-Chávez, H.; Miralrio, A.; Hernández-Rodríguez, Y.M.; Cruz-Martínez, H.; Pérez-Pérez, R.; Cigarroa-Mayorga, O.E. Needle- and Cross-Linked ZnO Microstructures and Their Photocatalytic Activity Using Experimental and DFT Approach. *Mater. Lett.* **2021**, *291*, 129474. [CrossRef]
30. van Mourik, T.; Bühl, M.; Gaigeot, M.-P. Density Functional Theory across Chemistry, Physics and Biology. *Philos. Trans. R. Soc. A Math. Phys. Eng. Sci.* **2014**, *372*, 20120488. [CrossRef] [PubMed]
31. Sibanda, D.; Oyinbo, S.T.; Jen, T.-C. A Review of Atomic Layer Deposition Modelling and Simulation Methodologies: Density Functional Theory and Molecular Dynamics. *Nanotechnol. Rev.* **2022**, *11*, 1332–1363. [CrossRef]
32. Brahim, N.; Thotagamuge, R.; Kooh, M.; Lim, C.; Syaahiran, M.; Usman, A.; Shahri, N.; Chou Chau, Y.-F.; Chou Chao, C.-T.; Chiang, H.-P.; et al. Enhanced CO Gas Sensing with DFT Optimized PbS Loading on ZnO and CrZnO Nanocomposites. *Sustainability* **2022**, *14*, 13978. [CrossRef]
33. Claeyssens, F.; Freeman, C.L.; Allan, N.L.; Sun, Y.; Ashfold, M.N.R.; Harding, J.H. Growth of ZnO Thin Films—Experiment and Theory. *J. Mater. Chem.* **2005**, *15*, 139–148. [CrossRef]
34. Kresse, G.; Furthmüller, J. Efficient Iterative Schemes for Ab Initio Total-Energy Calculations Using a Plane-Wave Basis Set. *Phys. Rev. B* **1996**, *54*, 11169–11186. [CrossRef] [PubMed]
35. Blöchl, P.E. Projector Augmented-Wave Method. *Phys. Rev. B* **1994**, *50*, 17953–17979. [CrossRef] [PubMed]
36. Perdew, J.P.; Burke, K.; Ernzerhof, M. Generalized Gradient Approximation Made Simple. *Phys. Rev. Lett.* **1996**, *77*, 3865–3868. [CrossRef] [PubMed]
37. Liechtenstein, A.I.; Anisimov, V.I.; Zaanen, J. Density-Functional Theory and Strong Interactions: Orbital Ordering in Mott-Hubbard Insulators. *Phys. Rev. B* **1995**, *52*, R5467–R5470. [CrossRef]
38. Ramanarayanan, P.; Sabirianov, R.F.; Cho, K. Point Defect Energetics in Silicon Using the LDA+ U Method. *arXiv* **2003**, arXiv:cond-mat/0310606.
39. Lee, Y.-S.; Peng, Y.-C.; Lu, J.-H.; Zhu, Y.-R.; Wu, H.-C. Electronic and Optical Properties of Ga-Doped ZnO. *Thin Solid Films* **2014**, *570*, 464–470. [CrossRef]
40. Ma, X.; Wu, Y.; Lv, Y.; Zhu, Y. Correlation Effects on Lattice Relaxation and Electronic Structure of ZnO within the GGA+U Formalism. *J. Phys. Chem. C* **2013**, *117*, 26029–26039. [CrossRef]
41. Monkhorst, H.J.; Pack, J.D. Special Points for Brillouin-Zone Integrations. *Phys. Rev. B* **1976**, *13*, 5188–5192. [CrossRef]
42. Ren, J.; Zhang, H.; Cheng, X. Electronic and Magnetic Properties of All 3d Transition-Metal-Doped ZnO Monolayers. *Int. J. Quantum Chem.* **2013**, *113*, 2243–2250. [CrossRef]
43. Tau, O.; Lovergine, N.; Prete, P. Adsorption and Decomposition Steps on Cu(111) of Liquid Aromatic Hydrocarbon Precursors for Low-Temperature CVD of Graphene: A DFT Study. *Carbon* **2023**, *206*, 142–149. [CrossRef]
44. Lu, G.-H.; Huang, M.; Cuma, M.; Liu, F. Relative Stability of Si Surfaces: A First-Principles Study. *Surf. Sci.* **2005**, *588*, 61–70. [CrossRef]

Disclaimer/Publisher's Note: The statements, opinions and data contained in all publications are solely those of the individual author(s) and contributor(s) and not of MDPI and/or the editor(s). MDPI and/or the editor(s) disclaim responsibility for any injury to people or property resulting from any ideas, methods, instructions or products referred to in the content.